Magnetoresistive junctions based on epitaxial graphene and hexagonal boron nitride

Oleg V. Yazyev* and Alfredo Pasquarello
Institute of Theoretical Physics, Ecole Polytechnique Fédérale de Lausanne (EPFL), CH-1015 Lausanne, Switzerland and Institut Romand de Recherche Numérique en Physique des Matériaux (IRRMA), CH-1015 Lausanne, Switzerland
(Received 29 May 2009; published 9 July 2009)

We propose monolayer epitaxial graphene and hexagonal boron nitride (*h*-BN) as ultimate thickness covalent spacers for magnetoresistive junctions. Using a first-principles approach, we investigate the structural, magnetic, and spin transport properties of such junctions based on structurally well-defined interfaces with (111) fcc or (0001) hcp ferromagnetic transition metals. We find low resistance area products, strong exchange couplings across the interface, and magnetoresistance ratios exceeding 100% for certain chemical compositions. These properties can be fine tuned, making the proposed junctions attractive for nanoscale spintronics applications.

DOI: 10.1103/PhysRevB.80.035408 PACS number(s): 72.25.−b, 73.43.Qt, 75.47.−m, 81.05.Uw

I. INTRODUCTION

Graphene (GR), a recently discovered two-dimensional form of carbon, has attracted unrivaled attention due to its unique physical properties and potential applications in electronics.[1,2] This nanomaterial is particularly promising for the field of spintronics, which exploits both the spin and the charge of electrons.[3–9] One fundamental spintronic effect is the magnetoresistance, the change in electric resistance as a function of the relative orientation, either parallel (P) or antiparallel (AP), of the magnetization of two ferromagnetic layers separated by a nonmagnetic spacer layer.[10] Achieving *high* MR ratios while keeping reasonably *low* electric resistance is crucial for many technological applications.[11] However, reaching this goal is currently hindered by material-specific restrictions such as the inability of producing well-ordered ferromagnet/spacer interfaces.[12,13]

Semimetallic graphene and its insulating counterpart, isostructural hexagonal boron nitride (*h*-BN), are promising spacers as epitaxial monolayers of these materials can be grown by means of chemical vapor deposition (CVD) on a broad variety of metallic substrates.[14–19] The quality of such epitaxial monolayers is very high and the covalent bonding network of both graphene and *h*-BN is perfectly preserved upon the bonding to the substrate. Moreover, the growth of graphene and *h*-BN on fcc(111) and hcp(0001) surfaces of ferromagnetic Co and Ni results in commensurate epitaxial layers due to the closely matching lattice constants.[14] This has led to a theoretical prediction of perfect spin filtering and, thus, to extremely high magnetoresistance ratios in such junctions based on multilayer graphene ($\geq$4 layers) and graphite.[20] However, the CVD growth on crystalline surfaces is self-inhibiting, that is, only one epitaxial layer can be grown. The deposition of ferromagnetic nanoparticles on top of epitaxial *h*-BN has also been demonstrated.[21,22] These interfaces further offer the opportunity of fine tuning their properties through the intercalation of other metals, such as Fe,[23] Cu,[24] and Au.[25]

In this work, we suggest the use of monolayer graphene and *h*-BN as *covalently* bonded spacer layers of minimal thickness in magnetoresistive junctions. Through first-principles calculations, we study the structural, magnetic, and spin transport properties of such junctions based on first-row ferromagnetic transition metals (TMs): natural hcp and fcc Co, fcc Ni, as well as intercalated fcc Fe. We show that the proposed magnetoresistive junctions realize low electric resistances, strong interlayer exchange couplings, and magnetoresistance ratios exceeding 100% for certain chemical compositions.

This paper is organized as follows. In Sec. II we describe our computational methodology, including the first-principles approach to electronic transport. In Sec. III we report the atomic structure and electronic properties of the considered magnetoresistive junctions. Particular attention is devoted to the interlayer exchange couplings. The results of electronic transport calculations are discussed in Sec. IV. Section V concludes our work.

II. COMPUTATIONAL METHODS

The electronic- and atomic-structure calculations were performed using the PWSCF plane-wave pseudopotential code of the QUANTUM-ESPRESSO distribution.[26] To achieve a good description of atomic structures, interlayer exchange couplings, and spin transport properties, we chose the Perdew-Burke-Ernzerhof exchange-correlation density functional.[27] Ultrasoft pseudopotentials were used to describe core-valence interactions.[28] The valence wave functions and the electron density were described by plane-wave basis sets with kinetic-energy cutoffs of 25 and 250 Ry, respectively.[29] The atomic structure of the magnetoresistive junctions considered in our work is illustrated in Fig. 1(a). Our investigation is restricted to only symmetric junctions, i.e., with the same metal on both sides of the spacer layer. Each ferromagnetic layer consisted of six atomic planes. The solutions for parallel and antiparallel relative spin orientations of these two layers were obtained by specifying appropriate initial orientations of the magnetic moments. The lateral unit cell of the studied interfaces is shown in Fig. 1(b). We considered bound configurations and determined the lowest-energy structures through the relaxation of atomic positions. For these configurations, we performed quantum transport calculations in the current perpendicular to plane configuration using the PWCOND code[30] of the same package. The scatter-

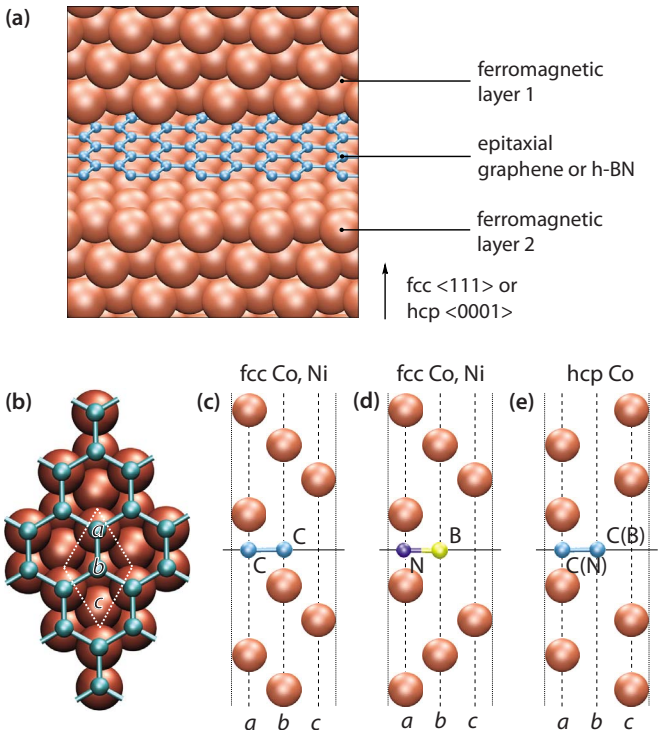

FIG. 1. (Color online) (a) Representation of the atomic structure of magnetoresistive junctions based on epitaxial monolayer graphene and *h*-BN. (b) Top view of graphene on (111) surface of fcc Co or Ni. The two-dimensional unit cell is indicated by dotted lines and the principal atomic positions are labeled. (c)–(e) Side views along the longest unit-cell diagonal of the lowest-energy interfaces formed by Co (hcp and fcc) and Ni (fcc) in combination with either monolayer graphene or *h*-BN.

ing region included the spacer monolayer and three adjacent monolayers of metal on both sides. We use the optimistic definition of the magnetoresistance ratio,

$$\mathrm{MR} = \frac{G_{\uparrow\uparrow} + G_{\downarrow\downarrow} - 2G_{\uparrow\downarrow}}{2G_{\uparrow\downarrow}} 100\%. \quad (1)$$

The spin-resolved quantum conductances G_σ for parallel ($\sigma = \uparrow\uparrow, \downarrow\downarrow$ for majority and minority spins, respectively) and antiparallel ($\sigma = \uparrow\downarrow$) configurations were calculated by integrating the corresponding $\mathbf{k}_\parallel$-dependent transmission probabilities $T^\sigma_{\mathbf{k}\parallel}$ evaluated on a uniform grid of 64×64 $\mathbf{k}$ points in the two-dimensional Brillouin zone.

III. ATOMIC AND ELECTRONIC STRUCTURE

To determine the lowest-energy structures of the junctions, we carried out structural relaxations for all possible stacking orders of the atomic planes in the vicinity of the spacer layer. The corresponding structures are shown in Fig. 1 for Co- and Ni-based junctions and summarized in Table I for all investigated chemical compositions. We find that both GR and *h*-BN bound to the TMs display short metal-carbon and metal-nitrogen distances (2.19–2.45 Å) comparable to the sum of the corresponding covalent bond radii. The thickness of the spacer layer is thus comparable to

TABLE I. Lowest-energy structures, interlayer exchange couplings ($\Delta E = E_\mathrm{P} - E_\mathrm{AP}$), spin-resolved quantum conductances ($G_{\uparrow\uparrow}$, $G_{\downarrow\downarrow}$, and $G_{\uparrow\downarrow}$), and magnetoresistance (MR) for the discussed GR and *h*-BN junctions. The notation for the stacking order is identical to the one in Fig. 1. The values of quantum conductances and interlayer exchange couplings are given per unit-cell area.

Junction	Stacking order	ΔE (meV)	$G_{\uparrow\uparrow}$ (e^2/h)	$G_{\downarrow\downarrow}$ (e^2/h)	$G_{\uparrow\downarrow}$ (e^2/h)	MR (%)
Fe|GR|Fe(fcc)	*cba*|*bac*	79	0.334	0.440	0.240	61
Fe|BN|Fe(fcc)	*cba*|*abc*	63	0.256	0.297	0.111	149
Co|GR|Co(fcc)	*bca*|*bca*	91	0.317	0.427	0.232	60
Co|BN|Co(fcc)	*bca*|*acb*	46	0.263	0.268	0.210	26
Ni|GR|Ni(fcc)	*bca*|*bca*	−18	0.352	0.587	0.402	17
Ni|BN|Ni(fcc)	*bca*|*acb*	−3	0.207	0.722	0.299	55
Co|GR|Co(hcp)	*aca*|*aca*	29	0.241	0.278	0.140	86
Co|BN|Co(hcp)	*aca*|*aca*	44	0.222	0.241	0.140	66

that of a single atomic plane of the ferromagnetic metal. For the Ni|GR|Ni(fcc) junction we find a Ni-C distance of 2.19 Å, which is close to 2.18 Å calculated for the graphene chemisorbed on the Ni(111) surface (i.e., Ni|GR system). The latter value is in good agreement with the experimental value of 2.16 ± 0.07 Å.[14]

We now turn to the electronic structure of these magnetoresistive junctions. Figure 2 shows the spin-resolved PDOS onto the light atoms (B, C, and N) of the fcc Co junctions. One can see that the characteristic "Dirac cone" density of states of the free-standing graphene is not preserved upon the formation of the Co|GR|Co(fcc) interface [Fig. 2(a)]. This is consistent with the theoretically predicted[20] and experimentally observed[31] strong hybridization between the electronic states of graphene and of the TM surface. Similarly, both B and N centered states fill the band gap of the insulating *h*-BN [Fig. 2(b)]. In both cases, we very similarly find significant contributions of the epitaxial layer states to the density of states at the Fermi level. In the parallel (antiparallel) configuration of the graphene-based junction, the induced magnetic moments on the carbon atoms in the unit cell are $-0.005\mu_\mathrm{B}$ ($0.081\mu_\mathrm{B}$ and $-0.081\mu_\mathrm{B}$). In the parallel configuration of the *h*-BN junction, the induced magnetic moments of N and B atoms are $0.029\mu_\mathrm{B}$ and $-0.065\mu_\mathrm{B}$, respectively. In the antiparallel configuration both vanish by symmetry.

The interlayer exchange coupling, the difference $\Delta E = E_\mathrm{P} - E_\mathrm{AP}$ between the energies of parallel and antiparallel configurations, is a manifestation of the superexchange mechanism. It achieves rather high values (cf. Table I) due to the ultimate thickness of the spacer layer. For Fe and Co, the antiparallel configuration is energetically favored. On the contrary, the parallel configuration is preferred for Ni. This intriguing crossover provides an opportunity for fine tuning the interlayer exchange by varying the chemical composition of the ferromagnetic layers.

IV. ELECTRONIC TRANSPORT

A. Role of spacer material

To understand the calculated quantum conductances and the resulting magnetoresistance ratios (cf. Table I), we ana-

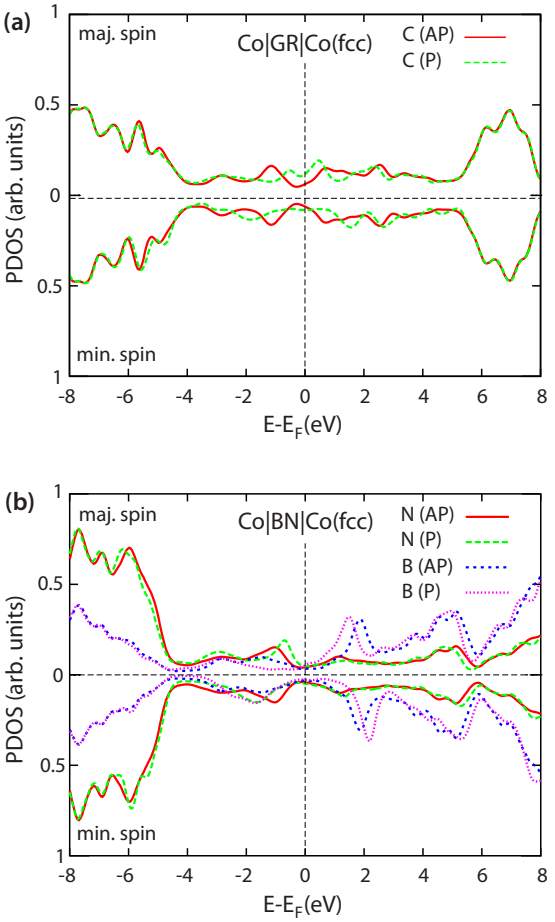

FIG. 2. (Color online) Spin-resolved projected density of states (PDOS) onto the atoms of the spacer layer, either (a) graphene or (b) *h*-BN, in the fcc Co junctions in their parallel and antiparallel configurations. The majority- and minority-spin labels refer to the parallel configuration; in the antiparallel arrangement the spin channels are equivalent.

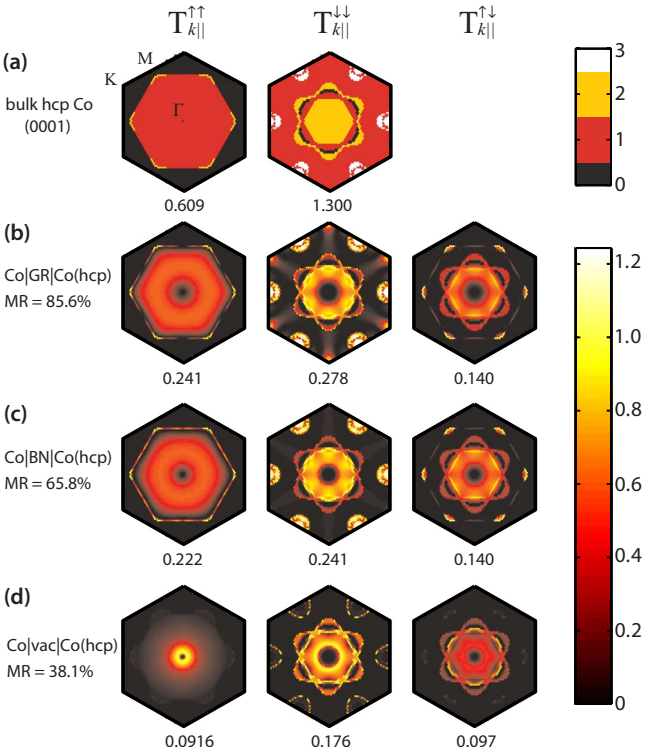

FIG. 3. (Color online) $\mathbf{k}_{\|}$-resolved conductance per unit cell (in units of e^2/h) through (a) bulk hcp Co along the (0001) direction, (b) Co|GR|Co(hcp), and (c) Co|BN|Co(hcp) junctions, and (d) a vacuum layer of equivalent thickness. The columns correspond to majority- and minority-spin channels of the parallel configuration and to one of the equivalent spin channels of the antiparallel configuration, respectively. Labels indicate the total conductances per unit-cell area.

lyzed the $\mathbf{k}_{\|}$-resolved transmission probabilities. First, we studied the effect of the spacer layer in hcp Co junctions which have the same lowest-energy structure for both graphene and *h*-BN [Fig. 3]. We found that both systems show strikingly similar $\mathbf{k}_{\|}$-resolved transmission probability maps [compare Figs. 3(b) and 3(c)] and, consequently, quantum conductances. The $T^{\uparrow\uparrow}_{\mathbf{k}\|}$ and $T^{\downarrow\downarrow}_{\mathbf{k}\|}$ maps reveal major features of the projected hcp Co Fermi surfaces for the free-electron-like majority spin and mostly *d*-symmetry minority-spin electrons [Fig. 3(a)], which are relevant to the quantum conductances of bulk metals.[32,33] The total transmission probabilities of the junctions in the parallel configurations constitute ~40% and ~20% of the Sharvin conductances[34] of bulk hcp Co along the (0001) direction. The quantum conductances in the antiparallel configuration are mostly determined by the overlap of $T^{\uparrow\uparrow}_{\mathbf{k}\|}$ and $T^{\downarrow\downarrow}_{\mathbf{k}\|}$. Their values are consequently lower ($G_{\uparrow\downarrow}$=0.140 e^2/h per unit cell for both spacer materials). The resulting magnetoresistance ratios are 86% and 66% for graphene and *h*-BN junctions. Thus, in the regime of ultimate thickness the transport properties are largely independent of the electronic structure differences of the two spacer materials. The role of a single layer of covalent spacer material consists in fixing a certain stacking order at the interface and in providing a medium for the abrupt change in magnetization in the antiparallel configuration. Due to the metallic nature of the spacer layers (cf. Fig. 2) such junctions possess low resistance area products ($<3\times10^{-15}$ Ωm^2) which makes them suitable for nanoscale spintronics applications such as the magnetic random access memories and spin-transfer nano-oscillators. We classify the present systems as *giant magnetoresistance* (GMR) junctions. This contrasts to the spin transport through a vacuum gap of the same thickness which shows $T^{\sigma}_{\mathbf{k}\|}$ decaying with $|\mathbf{k}_{\|}|$ [Fig. 3(d)], a characteristic feature of tunneling.[35] The magnetoresistance ratio is about twice smaller (38%) in the case of tunneling through a vacuum gap. This allows us to conclude that in the limit of ultimate thickness the GMR effect is more efficient than the tunneling magnetoresistance.

B. Role of ferromagnetic layers

Next, we studied the dependence of transport properties on the ferromagnetic metal by considering fcc Fe, Co, and Ni junctions in combination with *h*-BN. For all three metals, the majority-spin transmission in the parallel configuration $T^{\uparrow\uparrow}_{\mathbf{k}\|}$ undergoes little change along the Fe-Co-Ni series (Fig. 4). This behavior stems from the similarity of the corresponding

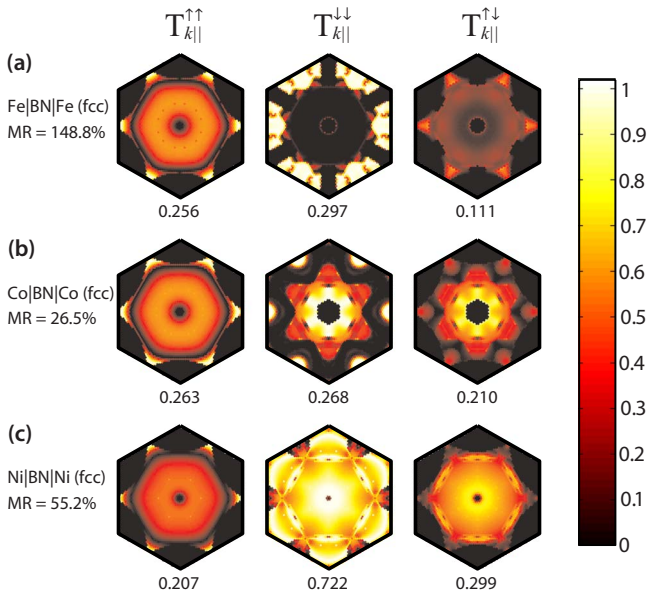

FIG. 4. (Color online) $\mathbf{k}_{||}$-resolved conductance per unit cell (in units of e^2/h) through fcc (a) Fe, (b) Co, and (c) Ni junctions based on monolayer *h*-BN. The columns correspond to majority- and minority-spin channels of the parallel configuration and to one of the equivalent spin channels of the antiparallel configuration, respectively. Labels indicate the corresponding total conductances per unit-cell area.

majority-spin Fermi surfaces of the bulk metals, which are formed by partially filled *s* bands. However, much larger differences are found for $T^{\downarrow\downarrow}_{\mathbf{k}||}$ involving the minority electrons. These reflect the drastically different Fermi surfaces resulting from the interplay between *s* and *d* states. The increase in $G_{\downarrow\downarrow}$ along the series can be attributed to the decrease in hybridization between *s* and *d* electrons upon the increase in *d* band filling:[36] in general, the free-electron-like *s* states show higher transmission probabilities. The $G_{\uparrow\downarrow}$ values are again determined by the overlap of $T^{\uparrow\uparrow}_{\mathbf{k}||}$ and $T^{\uparrow\downarrow}_{\mathbf{k}||}$ and tend to increase along the series. For the Fe|BN|Fe(fcc) junction, we find a magnetoresistance ratio of 150%: the largest value among the compositions studied.

Further search of magnetoresistive junctions with improved characteristics may consist in exploring asymmetric junctions and the intercalation of some other chemical elements at the interfaces. We here demonstrate the second possibility. It has been suggested that the incorporation of submonolayer quantities of Cu at the TM|GR_n interface would reduce undesired hybridization between the states of graphene and of the metal surface at the price of substantially decreasing the magnetoresistance ratios.[20] However, we find that the decoupling of the spacer layer from the metal surface does not necessarily imply the loss of magnetoresistance. This can be achieved by intercalating the metals from the middle of the transition metals series, e.g., Mn, which show reduced binding to carbon π systems.[37] Indeed, in the intercalated CoMn(1 ML)|GR|Mn(1 ML)Co(hcp) junction, the Mn-C distance increases to 2.95 Å and the interlayer exchange coupling decreases to 10 meV [to be compared with 29 meV for Co|GR|Co(hcp), cf. Table I]. Concurrently, the magnetoresistance ratio raises from 86% to 127%. The Mn layer is strongly spin polarized and antiferromagnetically coupled to hcp Co.

V. CONCLUSIONS

In conclusion, we propose epitaxially grown monolayer graphene and *h*-BN as ultimate thickness covalent spacers in transition-metal-based magnetoresistive junctions. Such junctions display well-ordered interfaces and can be produced through existing manufacturing processes. Their physical properties can be fine tuned in a broad range by varying the chemical composition. These systems show low resistance area products and typical GMR behavior with magnetoresistance ratios exceeding 100% for certain compositions. Both ferromagnetic and antiferromagnetic interlayer exchange couplings are found. These properties make the proposed junctions attractive for spintronics applications such as the magnetic random access memories and spin-transfer nano-oscillators.

ACKNOWLEDGMENTS

We acknowledge fruitful discussions with H. Brune, P. J. Kelly, and S. Rusponi. We would like to thank A. Smogunov for his help with the PWCOND code. The calculations were performed at the CSCS.

*Present address: Department of Physics, University of California, Berkeley, CA 94720, USA; yazyev@civet.berkeley.edu

[1] M. I. Katsnelson, Mater. Today **10**, 20 (2007).
[2] A. K. Geim and K. S. Novoselov, Nature Mater. **6**, 183 (2007).
[3] N. Tombros, C. Jozsa, M. Popinciuc, H. T. Jonkman, and B. J. van Wees, Nature (London) **448**, 571 (2007); N. Tombros, S. Tanabe, A. Veligura, C. Jozsa, M. Popinciuc, H. T. Jonkman, and B. J. van Wees, Phys. Rev. Lett. **101**, 046601 (2008).
[4] Y.-W. Son, M. L. Cohen, and S. G. Louie, Nature (London) **444**, 347 (2006).
[5] O. V. Yazyev and M. I. Katsnelson, Phys. Rev. Lett. **100**, 047209 (2008).
[6] F. Muñoz-Rojas, J. Fernández-Rossier, and J. J. Palacios, Phys. Rev. Lett. **102**, 136810 (2009).
[7] O. V. Yazyev and L. Helm, Phys. Rev. B **75**, 125408 (2007); O. V. Yazyev, Phys. Rev. Lett. **101**, 037203 (2008).
[8] W. L. Wang, S. Meng, and E. Kaxiras, Nano Lett. **8**, 241 (2008); O. V. Yazyev, W. L. Wang, S. Meng, and E. Kaxiras, *ibid.* **8**, 766 (2008); W. L. Wang, O. V. Yazyev, S. Meng, and E. Kaxiras, Phys. Rev. Lett. **102**, 157201 (2009).
[9] O. V. Yazyev, Nano Lett. **8**, 1011 (2008).
[10] C. Heiliger, P. Zahn, and I. Mertig, Mater. Today **9**, 46 (2006).
[11] C. Chappert, A. Fert, and F. N. Van Dau, Nature Mater. **6**, 813 (2007).

[12] S. Yuasa, T. Nagahama, A. Fukushima, Y. Suzuki, and K. Ando, Nature Mater. **3**, 868 (2004).
[13] C. Heiliger, P. Zahn, B. Y. Yavorsky, and I. Mertig, Phys. Rev. B **73**, 214441 (2006).
[14] C. Oshima and A. Nagashima, J. Phys.: Condens. Matter **9**, 1 (1997).
[15] S. Berner, M. Corso, R. Widmer, O. Groening, R. Laskowski, P. Blaha, K. Schwarz, A. Goriachko, H. Over, S. Gsell, M. Schreck, H. Sachdev, T. Greber, and J. Osterwalder, Angew. Chem., Int. Ed. **46**, 5115 (2007).
[16] J. Coraux, A. T. N'Diaye, C. Busse, and T. Michely, Nano Lett. **8**, 565 (2008).
[17] A. L. Vázquez de Parga, F. Calleja, B. Borca, M. C. G. Passeggi, J. J. Hinarejos, F. Guinea, and R. Miranda, Phys. Rev. Lett. **100**, 056807 (2008).
[18] P. W. Sutter, J.-I. Flege, and E. A. Sutter, Nature Mater. **7**, 406 (2008).
[19] D. Martoccia, P. R. Willmott, T. Brugger, M. Bjorck, S. Gunther, C. M. Schleputz, A. Cervellino, S. A. Pauli, B. D. Patterson, S. Marchini, J. Wintterlin, W. Moritz, and T. Greber, Phys. Rev. Lett. **101**, 126102 (2008).
[20] V. M. Karpan, G. Giovannetti, P. A. Khomyakov, M. Talanana, A. A. Starikov, M. Zwierzycki, J. van den Brink, G. Brocks, and P. J. Kelly, Phys. Rev. Lett. **99**, 176602 (2007); V. M. Karpan, P. A. Khomyakov, A. A. Starikov, G. Giovannetti, M. Zwierzycki, M. Talanana, G. Brocks, J. van den Brink, and P. J. Kelly, Phys. Rev. B **78**, 195419 (2008).
[21] W. Auwärter, M. Muntwiler, T. Greber, and J. Osterwalder, Surf. Sci. **511**, 379 (2002).
[22] J. Zhang, V. Sessi, C. H. Michaelis, I. Brihuega, J. Honolka, K. Kern, R. Skomski, X. Chen, G. Rojas, and A. Enders, Phys. Rev. B **78**, 165430 (2008).
[23] Yu. S. Dedkov, M. Fonin, U. Rudiger, and C. Laubschat, Appl. Phys. Lett. **93**, 022509 (2008).
[24] Yu. S. Dedkov, A. M. Shikin, V. K. Adamchuk, S. L. Molodtsov, C. Laubschat, A. Bauer, and G. Kaindl, Phys. Rev. B **64**, 035405 (2001).
[25] A. Varykhalov, J. Sanchez-Barriga, A. M. Shikin, C. Biswas, E. Vescovo, A. Rybkin, D. Marchenko, and O. Rader, Phys. Rev. Lett. **101**, 157601 (2008).
[26] Quantum-ESPRESSO is a community project for high-quality quantum-simulation software, based on density-functional theory, and coordinated by Paolo Giannozzi. See http://www.quantum-espresso.org and http://www.pwscf.org
[27] J. P. Perdew, K. Burke, and M. Ernzerhof, Phys. Rev. Lett. **77**, 3865 (1996).
[28] D. Vanderbilt, Phys. Rev. B **41**, 7892 (1990).
[29] A. Pasquarello, K. Laasonen, R. Car, C. Lee, and D. Vanderbilt, Phys. Rev. Lett. **69**, 1982 (1992); K. Laasonen, A. Pasquarello, R. Car, C. Lee, and D. Vanderbilt, Phys. Rev. B **47**, 10142 (1993).
[30] A. Smogunov, A. Dal Corso, and E. Tosatti, Phys. Rev. B **70**, 045417 (2004); H. Joon Choi and J. Ihm, *ibid.* **59**, 2267 (1999).
[31] A. Grüneis and D. V. Vyalikh, Phys. Rev. B **77**, 193401 (2008).
[32] K. M. Schep, P. J. Kelly, and G. E. W. Bauer, Phys. Rev. B **57**, 8907 (1998).
[33] M. Zwierzycki, P. A. Khomyakov, A. A. Starikov, K. Xia, M. Talanana, P. X. Xu, V. M. Karpan, I. Marushchenko, I. Turek, G. E. W. Bauer, G. Brocks, and P. J. Kelly, Phys. Status Solidi B **245**, 623 (2008).
[34] Yu. V. Sharvin, Zh. Eksp. Teor. Fiz. **48**, 984 (1965) [Sov. Phys. JETP **21**, 655 (1965)].
[35] K. D. Belashchenko, E. Y. Tsymbal, M. van Schilfgaarde, D. A. Stewart, I. I. Oleinik, and S. S. Jaswal, Phys. Rev. B **69**, 174408 (2004).
[36] I. I. Mazin, Phys. Rev. Lett. **83**, 1427 (1999).
[37] R. Pandey, B. K. Rao, P. Jena, and M. A. Blanco, J. Am. Chem. Soc. **123**, 3799 (2001).